Astron. Astrophys. 363, 1155–1165 (2000)

ASTRONOMY AND ASTROPHYSICS

Statistical study of polarization of light scattered by rough grains

I. The method with preliminary results

K. Chamaillard and J.-P.J. Lafon

Observatoire de Meudon, DASGAL, 92195 Meudon, France

Received 18 November 1999 / Accepted 19 July 2000

Abstract. In order to quantify the effects of shape of grains on their optical properties, we use a new statistical approach to study the effects of roughness on the degree of linear polarization.

In this approach, we compute the degree of linear polarization of light scattered by a rough grain. The roughness is obtained by a random depletion of the surface of an homogeneous sphere. The analysis of the results is achieved through a specific statistical method: the probability density function of the linear polarization P_l is estimated by a Gaussian kernel method. This method allows the characterization of effects specifically due to the roughness.

The grain is described by the Discrete Dipole Approximation (DDA) (Draine 1988). We present the preliminary results for a spherical grain of water ice with radius $a_{\rm eff} \simeq 0.3\mu m$ which is comparable to the incident wavelength $\lambda = 1.88\mu m$ where water ice is non-absorbing.

The effect of grains roughness on polarization can be distinguished from the effects of volume in several different ways. The shape of the density function of the polarization is found to be non-symmetrical to the mean value of P_l and non-unimodal for several scattering angles. We compare the mean value of the linear polarization deduced from the probability density function to the value obtained from a mass equivalent sphere and from the core sphere. We present the effects of roughness for various scattering angles.

Key words: polarization – scattering – ISM: dust, extinction – stars: circumstellar matter

1. Introduction

The characteristics of circumstellar and interstellar dust grains depend generally on three sets of parameters. Each set of parameters is necessary to describe each characteristic of the grains: their size, morphology and composition. These parameters are determined by comparison between observations and theoretical models (Lafon & Berruyer 1991). In general, these parameters cannot be derived directly from observations, and there remain partly *adhoc* free parameters in theoretical computation of optical properties of grains (extinction, absorption and scattering cross sections, and also, polarization of light radiated by dust). Among these optical properties, the scattering efficiencies and the degree of polarization are very sensitive to the structure and shape of the grains (Bohren & Huffman 1983).

Several approaches have been proposed to model dust grains. One of the most often applied models consists of a power-law size distribution of homogeneous spherical and bare grains of different materials (Mathis et al. 1977, hereafter MRN). Unfortunately, we cannot expect grains formed under complicated processes to be spherical or to have a regular shape. More recent models use inhomogeneous grains in shape and/or composition, for example core/mantle grains (Hagen et al. 1983) or porous grains. The latter are thought to be formed through coagulation rather than by accretion (Mathis & Whiffen 1989), which implies a high level of porosity of the grains. Principal models of these grains are grains with random inclusions (e.g. Wolff et al. 1994; Lumme & Rahola 1994; Perrin & Sivan 1991), although fractal models are sometimes preferred (e.g. Ossenkopf 1993; Stognienko et al. 1995; Kozasa et al. 1993).

To calculate the optical properties of such grains, two approximations are currently available. One is the Discrete Dipole Approximation (DDA) introduced by Purcell & Pennypacker (1973), and improved by Draine (1988). In this model, the grain is replaced by a set of electric dipoles which are macroscopic compared to atoms and microscopic compared to the size of the grain. The other approximation is Effective-Medium Theories (EMT) where the dielectric functions of the porous grain is replaced by an effective function, see for example Bohren & Huffman (1983). As the latter approximation is not suitable to describe the special effect of grain morphology and in particular, surface roughness (Ossenkopf 1991), we use the DDA to study the effect of shape of grains.

On the other hand, porous grains as well as fractal aggregates have a fluffy structure but a rough surface that has to be taken into account in calculations of the scattering properties of the grains (Ossenkopf 1991). Moreover, porous internal structure can modify the measured dielectric functions of the grains compared to the optical bulk constants. In order to fully separate the effects of internal structure from the effects of shape, we keep the size and composition of grain constant to study in detail the effect of surface roughness on the linear polarization of the scattered light of an initially spherical grain.

Send offprint requests to: K. Chamaillard

A review of previous work on roughness and a description of our approach to the problem is given in Sect. 2. In Sect. 3, we review the characteristics of the model (DDA) used for our statistical simulations and emphasize why it is convenient for our study. We also describe the roughness modeled. In Sect. 4, we present in detail the new statistical method applied: a Gaussian kernel method from which we deduce the probability density function of the polarization which characterizes some typical roughness of grains. We display and discuss our results obtained for one wavelength where water ice is non-absorbing. Sect. 5 is devoted to a general conclusion including possible development of this approach.

2. Previous works and description of the new approach

2.1. Review of the problem and previous works on roughness

The problem of the scattering of light by particles of small size compared to the incident wavelength (or of the same order) is usually solved using the classical equations of electromagnetism. To solve Maxwell's equations, the crucial problem is that of the boundary conditions (Mugnai & Wiscombe 1980) which characterize the grain surface. The only cases for which we can derive the analytical solutions are those where the grains have exactly the same geometry and symmetry as the coordinate system chosen to develop the equations, among which Mie's spheres are a particular case.

On the other hand, size, morphology and composition of dust grains cannot be directly inferred from a comparison between observations and theoretical models. This inversion problem cannot be easily solved for several reasons. One reason is that the equations do not depend linearly on these parameters, at least through the refraction index, and then, the solution is probably not unique. A specific grain candidate with a particulate size, shape, and composition can as well reproduce the results as another grain candidate with different parameters. Another reason is that these parameters characterizing the grain cannot be treated as independent variables, as is generally assumed. For instance : the optical constants of the material depend on the morphology and structure of the grain. One approach devoted to the effect of internal structure is based on the applicability of EMT-type solutions as described in Wolff et al. (1994, 1998); Stognienko et al. (1995); Ossenkopf (1991); Rouleau (1996).

In addition to the internal structure that affects the optical properties, grains also have a rough surface which is rarely studied in models. One approach (Mugnai & Wiscombe 1980; Mishchenko & Hovenier 1995) uses expansion with Chebyshev's polynomials to deform a sphere. Despite the advantage that this method does not use any approximations, the shape of the grain is still too regular to represent a real grain.

Another approach used by Perrin & Sivan (1991) consists of removing random elements of matter from the surface of a sphere. In their definition of roughness, deep holes on the grain can reach up to 70% of the initial sphere radius. In that case, we consider that the internal structure of the grain is modified so that the effect of roughness cannot be separated from those of volume.

While in Perrin & Sivan (1991) the radius of the sphere is comparable to the incident wavelength, McGuire & Hapke (1995) have studied the optical effects of rough spheres with a size much larger than the incident wavelength, so that the irregularities of the sphere are also very large compared to the incident wavelength. In our case, we are mainly interested in the effects of roughness of particles with size comparable to the incident wavelength, for Mie's theory to be valid.

The above works on porous and/or rough grains then intend to simulate a collection of grains. There are generally two ways to model a collection of roughly identical grains with a uniform distribution in space: one is based on simulation of numerous grains with the same fractal dimension or same degree of porosity and the other is based on orientation averaging of one grain. Whereas it is commonly admitted that these two approaches are equivalent (Lumme & Rahola 1994), only the second one describes a collection of randomly oriented identical grains (Bohren & Huffman 1983). Nevertheless, both models will result in depolarization of light.

Measurements of polarization of starlight in the interstellar medium require that a significant fraction of interstellar grains are aligned (Draine & Weingartner 1997). In this case, averaging over one angle is required to take into account the degree of freedom still available along the line of sight. In our case, we will restrict the discussion to one grain that would represent the case of a perfect alignment of the particles. As our goal is to study in detail the effects of roughness of dust grains on polarization with the statistical method developed here after, it is necessary to first restrict this discussion to a single grain in order to point out some specific feature before considering a collection of grains (which will be done in a forthcoming paper).

Previous works have applied different statistical models for the scattering of light by irregular particles. Drossart (1990) proposed a concept of partial coherence of the individual spherical harmonics, assuming a Gaussian distribution for the coherence functions to describe effects of roughness. While the main goal of this work is to provide a new model to approximate scattering by irregular particles, we do not present a model but rather a method to study in detail the dependence of the polarization on the shape of the grains, for which roughness is a first step.

Muinonen (1996), Peltoniemi et al. (1989), Muinonen (1998) and Muinonen & Lagerros (1998) used multivariate lognormal statistics, and Schiffer (1985) Gaussian statistics, to deform stochastically large spheres. Then, scattering efficiencies (albedo, polarization) are derived through Monte-Carlo simulations or after randomly orienting grains. Here, we adopt a different statistical point of view: not only is the surface roughness described by a random variable but also the observable (the linear polarization), which is then analyzed using a specific statistical method.

2.2. Description of the statistical approach

To quantify the effects of morphology, a comparison with spheres described using Mie's theory came naturally as a start-

ing point. We use a uniform law of exclusion to carve the surface of an homogeneous sphere for which we compute the linear polarization for each simulation of roughness. In order to define the roughness applied on the sphere we need to introduce a term that we call the 'thickness' of the surface of the sphere. The surface of the sphere is defined by the external shell of the sphere which has a thickness estimated to about $0.1\,a_{\rm eff}$ (where $a_{\rm eff}$ is the radius of the initial sphere). Thus, the elements of matter removed from the surface have a fixed height equal to $0.1\,a_{\rm eff}$.

Then, we define the degree of roughness by the ratio of the elements of matter removed to the initial number of elements of matter which compose the surface of the grain. The chosen degree of roughness applied here is set to 30%, and lies between a few percent that wouldn't be enough to characterize a significant effect and 50% that begins to represent a high degree of roughness. We will see in Sect. 4 that this chosen degree effectively permits us to quantify an effect of roughness.

Only the spatial distribution of holes changes from one simulation to another, and is characterized by the uniform law. For each rough sphere, we calculate the degree of linear polarization for various scattering angles. We repeat the simulation for $n = 1000$ times with the same degree of roughness. This gives us $n = 1000$ values of linear polarization which are then set as a random variable. A large number of simulations was needed to obtain a sufficient number of significantly different values in order to apply a Gaussian kernel method to this set of random variables. From this method, we can derive, for each scattering angle, the probability density function of the linear polarization which contains all the information about the roughness applied (see Sect. 4).

In this first paper, we present the preliminary results of this method for an initially spherical homogeneous grain. We consider a typical interstellar grain composed of water ice with size $a_{\rm eff} \simeq 0.3\mu$m (MRN, Pendleton et al. 1990) and size parameter $\mathrm{x} = 2\pi a_{\rm eff}/\lambda \simeq 1$ which corresponds to an incident wavelength $\lambda \simeq 1.88\mu$m.

3. Numerical method

3.1. Numerical modeling and accuracy of the model DDA

We performed the numerical simulations using the DDA model.

In the model, the grain is replaced by a set of electric dipoles which are small compared to the wavelength and the grain size. The dipoles are larger than atomic dipoles in order for the classical equations of electromagnetism to be valid. The main approximation of this method is that the electric dipole interactions are taken into account in the limit of long-wavelengths and large distance between dipoles. Then, the dipoles are located at the nodes of a cubic array (Draine 1988).

The DDA code internally computes the scattering properties of the dipole array in terms of a complex scattering matrix, so that the scattered electric field $\mathbf{E}_s$ is related to the incident electric field $\mathbf{E}_{\rm inc}$ by a 2×2 complex *amplitude scattering matrix* $\mathcal{S}$. The elements of $\mathcal{S}$ are a function of θ_s the scattering angle, and ϕ_s the azimuth angle, and depend on the characteristic parameters of the grain (size, composition, shape). $\mathbf{E}_{\rm inc}$ and $\mathbf{E}_s$ (respectively incident and scattered field) are split in components parallel and perpendicular to the scattering plane (see Fig. 1). In Fig. 1 the incident wave vector $\mathbf{k}$ is propagating along the z-axis.

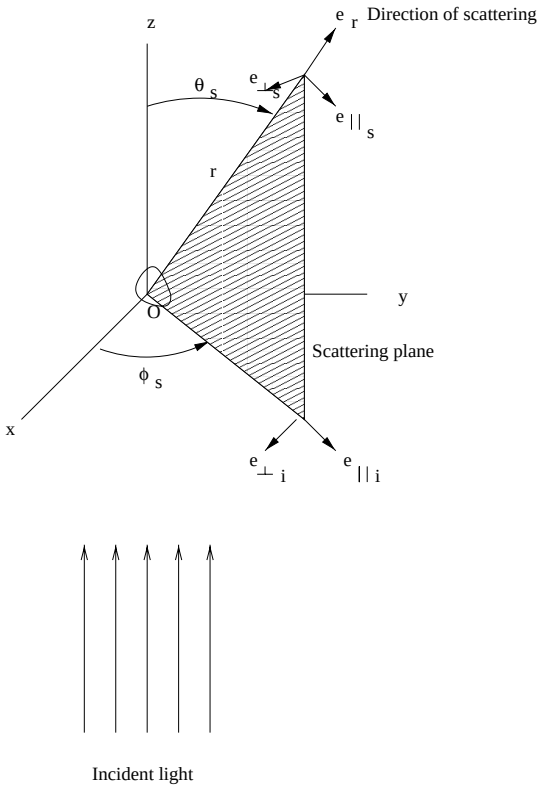

Fig. 1. Scattering by a grain of any shape.

It is more convenient to describe the scattering properties in terms of the 4×4 Mueller matrix S_{ij} connecting the Stokes parameters $(I_{\rm inc}, Q_{\rm inc}, U_{\rm inc}, V_{\rm inc})$ and (I_s, Q_s, U_s, V_s) of the incident and scattered radiation at the distance **r**:

$$\begin{pmatrix} I_s \\ Q_s \\ U_s \\ V_s \end{pmatrix} = \frac{1}{k^2 r^2} S_{ij} \begin{pmatrix} I_{\rm inc} \\ Q_{\rm inc} \\ U_{\rm inc} \\ V_{\rm inc} \end{pmatrix} , \tag{1}$$

where the S_{ij} are related to the amplitude scattering matrix elements $\mathcal{S}$ through analytical relations (Bohren & Huffman 1983) which are straightforwardly implemented in the code.

The quantity we are interested in is the degree of linear polarization P_l of the scattered light, which is defined by:

$$P_l = \frac{({Q_s}^2 + {U_s}^2)^{1/2}}{I_s} , \tag{2}$$

which in the case of incident unpolarized light is reduced to:

$$P_l = \frac{(S_{21}^2 + S_{31}^2)^{1/2}}{S_{11}} , \tag{3}$$

The linear polarization P_l is then angle (θ_s,ϕ_s) dependent.

The main advantage of the DDA is that it is a flexible method regarding the geometry of the target. This approximation of

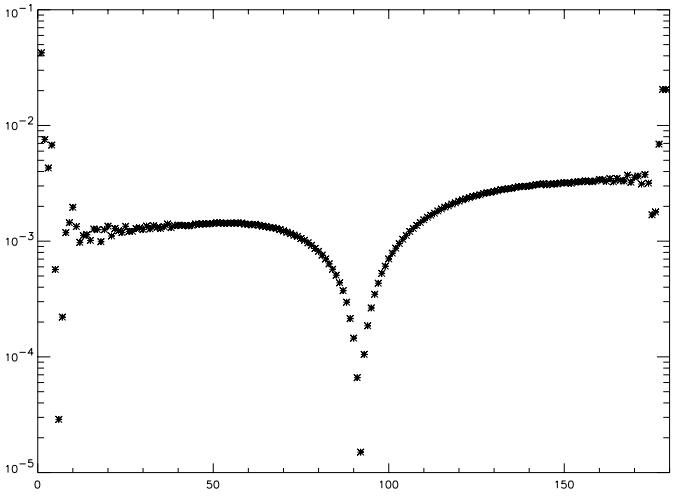

Fig. 2. Relative error of P_l calculated by the DDA method in comparison with Mie's theory versus the scattering angle θ_s

a continuous target is limited only by the condition that the distance between two neighboring dipoles d be small compared to, first, any structural lengths in the target, and second, the wavelength λ of the incident wave. Furthermore, d has to be small compared to the wavelength within the grain and be small also compared to the attenuation of the electromagnetic wave. This can be written by:

$$|m|kd \ll 1, \tag{4}$$

where m is the complex refractive index of the material and k the wave number $2\pi/\lambda$.

A validity criterion is then given by the dimensionless parameter Δ (Draine & Goodman 1993; Draine & Flatau 1994):

$$|m|kd < \Delta. \tag{5}$$

If the target is represented by an array of N dipoles large enough, located on a cubic lattice with lattice spacing d, then the target volume can be taken as $V = Nd^3$. If the size of the target is characterized by an effective radius $a_{\rm eff} \equiv (3V/4\pi)^{1/3}$ of an equal volume sphere, then the size parameter x can be related to N and $|m|kd$ by:

$$x \equiv \frac{2\pi a_{\rm eff}}{\lambda} = \left(\frac{3}{4\pi}\right)^{1/3} \cdot \frac{N^{1/3}}{|m|} \cdot |m|kd\,, \tag{6}$$

which with 5 gives:

$$|m|kd = \left(\frac{4\pi}{3}\right)^{1/3} \cdot \frac{x|m|}{N^{1/3}} < \Delta\,, \tag{7}$$

Numerical studies (Draine & Goodman 1993; Draine & Flatau 1994) show that a stringent criterion with $\Delta = 0.5$ in relation (5) should be satisfied for accurate calculations.

Criterion (7) is easily satisfied in calculations, with $x \simeq 1$ and $|m| \simeq 1$, if $N \geq 32$.

Nevertheless, the DDA method introduces some artificial granularity in modeling a spheroïdal shape on a cubic array (Draine & Flatau 1994): a numerical artifact is caused by the dipoles in regions near the target boundaries. To study the particular effect of the roughness of grains on scattering, and in order to reduce this numerical artifact, we use the largest number of dipoles allowed by the computer memory. However, the choice of the number of dipoles depends on the acceptable CPU time, and also on the quantum limit reached by the dipoles for a given V. We fix the quantum limit to 100Å, i.e. 0.01μm. We take $d = 0.01\mu$m in our calculations as the lower limit acceptable for d. This allows us to use a number of dipoles for the sphere equal to $N = 65752$ (for a $512Mo$ memory) to describe an initial sphere with radius $a_{\rm eff} = 0.3\mu$m. We take the size parameter $x = 2\pi a_{\rm eff}/\lambda \simeq 1$ and consider a typical astrophysical grain of ice at the wavelength $\lambda = 1.88\mu$m. Under such conditions, the complex refractive index is $m = 1.29 + 0.0002i$ (Pollack et al. 1991).

All these values lead to $\Delta \simeq 5.10^{-2}$ which is a more satisfactory criterion of (4) than $\Delta = 0.5$.

We verify the accuracy of this method by comparison with the results of Mie's theory with spherical grains. We have compared the degree of linear polarization computed with the DDA method to the theoretical value obtained with Mie's theory in the case of spheres: $\Delta P_l = P_l(DDA) - P_l(Mie)$. Fig. 2 represents the relative error of the linear polarization $\Delta P_l/P_l$ versus the scattering angle θ_s. The results of Mie's theory have been obtained with the numerical code given in Appendix A of Bohren & Huffman (1983). The parameters we used in the DDA model for this comparison are: $a_{\rm eff} = 0.3\mu$m, $\lambda = 1.88\mu$m (which give $x \simeq 1$), $m = 1.29 + 0.0002i$ for water ice at this wavelength, and $N = 65\,752$ dipoles in the sphere. We find that the fractional error due to the approximation is less than about 0.1% for any scattering angle greater than about $5°$, and is very small near $\theta_s = 90°$ ($\Delta P_l/P_l \simeq 10^{-3}\%$). We note that the error is approximately a constant for $\theta_s \in [10°; 80°] \cup [100°; 170°]$. We also found that this method tends to overestimate the polarization of the sphere in the range [10°;80°] and underestimate the polarization in the range [100°;170°]. We consider that the error of the model is systematic over both intervals.

3.2. Generation of the grain roughness

We start from a spherical grain and remove dipoles from its surface only. The removed dipoles will be counted as holes that will model a certain roughness. The depth of the surface of the spherical grain is defined as about 10% of $a_{\rm eff}$ which corresponds to 3 layers of dipoles. The dipoles are never removed from layers deeper than these three layers. All holes are then three dipoles deep. The width of each element of matter removed is fixed to one dipole, which then corresponds to the distance d between two dipoles. As the dipoles are removed at random, the average width of holes on the surface is larger than one dipole. Then, the degree of roughness is defined as the ratio of the total number of dipoles removed to the initial number of dipoles on the surface. As the depth of holes is fixed for all holes, and corresponds to the thickness of the surface we have defined, we take into ac-

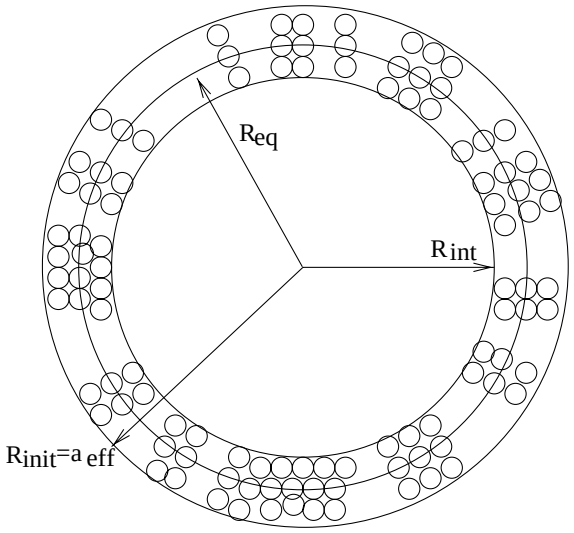

Fig. 3. Schema of the three spheres: $R_{\rm init} \equiv a_{\rm eff}$ is the radius of the initial sphere, $R_{\rm eq}$ that of the sphere with mass equivalent to that of the remaining dipoles, and $R_{\rm int}$ that of the interior sphere. Note that the dipoles represented by the small circles are out of scale for better clarity.

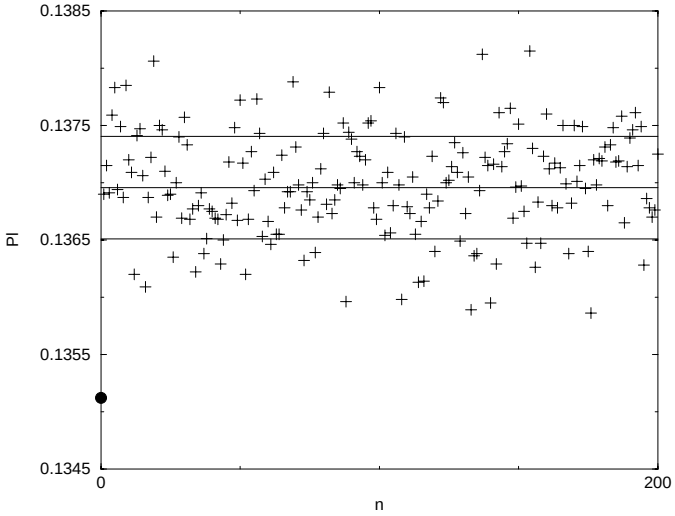

Fig. 4. Degree of linear polarization versus the number n of simulations, for $(\theta_s = 30°, \phi_s = 0°)$. The horizontal lines represent the average value and the mean square. The filled circle corresponds to $P_{l,0}$.

count only the outer layer for the determination of the degree of roughness. We fix the degree of roughness to 30%.

With a total number of dipoles within the sphere equal to $N = 65752$, the number of dipoles of the outer layer is only $N_S = 7896$. We randomly remove about 30% of these N_S dipoles, say, $N_H = 2732$ that are now counted as holes on the surface with a depth of $3d$.

As we intend to repeat the simulations $n = 1000$ times, a large number of dipoles is necessary to ensure that the spatial distribution will be different from one simulation to another.

4. Results and discussion

To quantify statistically the effects of roughness on polarization we compute the degree of linear polarization P_l for each stochastic simulation. We made $n = 1000$ stochastic simulations which give a set of the random variable P_l: $P_{l,1} \cdots P_{l,n=1000}$. For instance, Fig. 4 shows P_l versus the number of stochastic simulations n, reduced to $n = 200$ stochastic removal processes for better clarity. In Fig. 4 we have plotted the average value of the polarization in the $n = 1000$ simulations $\langle P_l \rangle_n$, and the standard deviation σ. We stress on the fact that we do not average the intensity involved in the definition of polarization but average directly the polarization $P_l(\theta_s, \phi_s)$ over the $n = 1000$ simulations. From a physical point of view, this average ($\langle P_l \rangle_n$) will never represent the net polarization of a collection of grains for which only the individual intensity can be added, but the information we get from this particular study will represent the specific effect of roughness on polarization.

The average value $\langle P_l \rangle_n$ can have no meaning although usually used without verifying its validity. In order to determine whether the average value $\langle P_l \rangle_n$ is physically relevant for use in computations, we have to calculate the probability density function of P_l. In addition to the mean value, the probability density function contains the number of modes, i.e., the number of maxima of the function. Even in the case of only one maximum, if the mean value doesn't coïncide with the maximum of the function, i.e. the most probable value, the average value has no physical meaning. If the density function exhibits more than one maximum, the interpretation becomes difficult.

In practice, we do not know the probability function of the random variable. The only value that is available is the empirical repartition function which, we remind, corresponds to the integrated probability density function over a restricted interval. Then, the probability density function deduced from the empirical repartition function will be a sum of Dirac functions. Nevertheless, if the number of values is large enough, one can approximate the density function by a continuous function using a kernel method. The details concerning the construction of this method is given in Appendix. Here, we choose a Gaussian kernel method.

We have calculated the probability density function of the linear polarization P_l for several scattering angles θ_s in the interval $[0°; 360°]$ *and* for 3 values of ϕ_s: $0°, 30°, 90°$ (only results for $\phi_s = 0°$ and $\phi_s = 90°$ are shown). Fig. 5 to Fig. 19 show the probability density functions of P_l obtained for several scattering angles. We have used exactly the same scale along the x-axis for all these figures.

The general aspect of the density function shows the specific effect of roughness at least in two ways: the first one is the shape of the density function which characterizes the type of roughness applied and, among other things, contains the number of maxima. The other way is the highest maximum which reflects the mean effect of roughness on P_l. What first appears is that the density functions are rarely symmetrical around the most probable value, i.e. the principal mode of P_l, in view of the randomness of the roughness. Moreover, in some cases, a

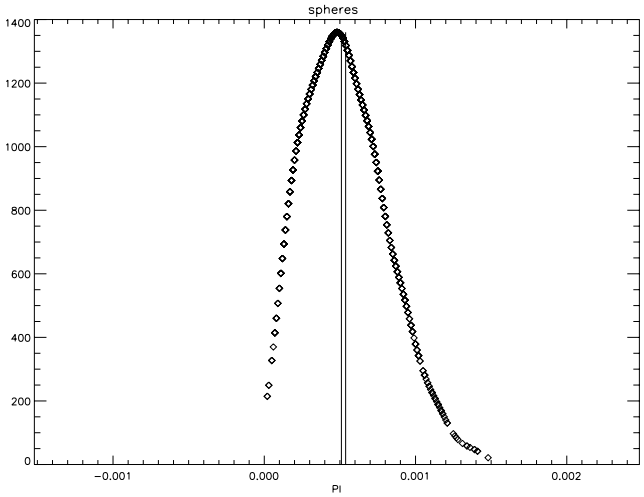

Fig. 5. Density function of linear polarization P_l for $(\theta_s = 0°, \phi_s = 0°)$. $P_{l,0} = P_{l,\mathrm{eq}} = P_{l,\mathrm{int}} = 0$. The vertical lines correspond to $\langle P_l \rangle_n$ and the median value.

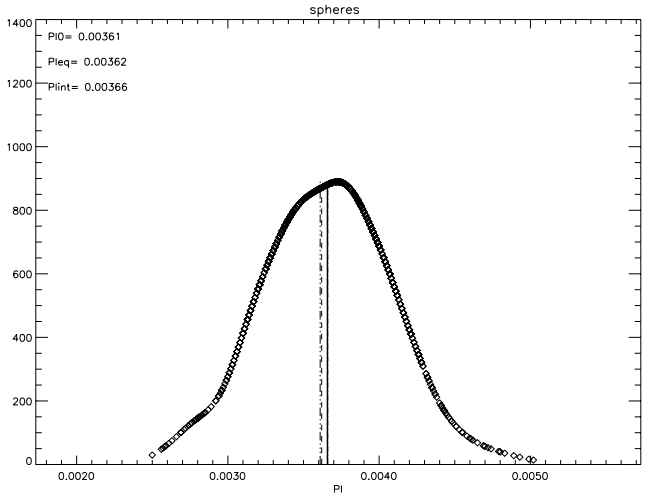

Fig. 7. Density function of linear polarization P_l for $(\theta_s = 5°, \phi_s = 90°)$. $P_{l,0}$:– · · · –, $P_{l,\mathrm{eq}}$:– –, $P_{l,\mathrm{int}}$:– · –. The vertical lines correspond to $\langle P_l \rangle_n$ and the median value.

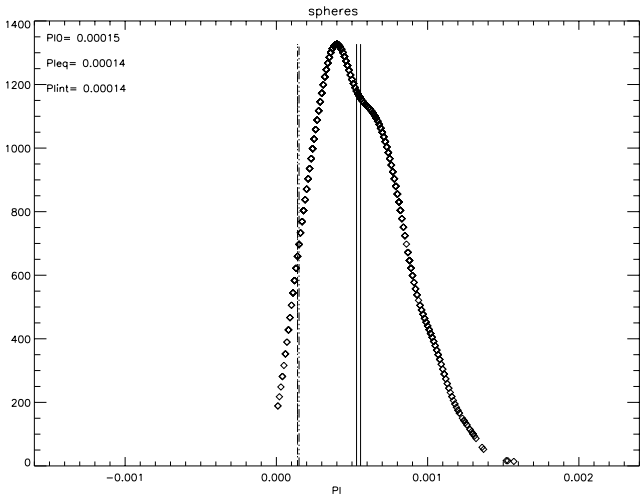

Fig. 6. Density function of linear polarization P_l for $(\theta_s = 1°, \phi_s = 0°)$. $P_{l,0}$:– · · · –, $P_{l,\mathrm{eq}}$:– –, $P_{l,\mathrm{int}}$:– · –. The vertical lines correspond to $\langle P_l \rangle_n$ and the median value.

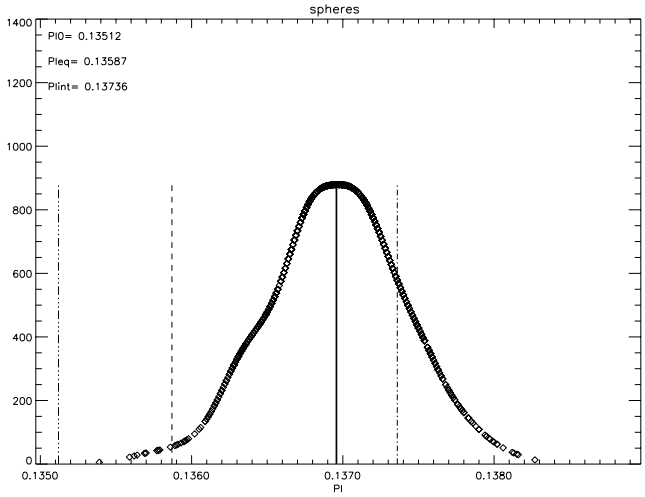

Fig. 8. Density function of linear polarization P_l for $(\theta_s = 30°, \phi_s = 0°)$. $P_{l,0}$:– · · · –, $P_{l,\mathrm{eq}}$:– –, $P_{l,\mathrm{int}}$:– · –. The vertical lines correspond to $\langle P_l \rangle_n$ and the median value.

secondary maximum clearly appears, as for instance at the scattering angle $\theta_s = 150°(\phi_s = 0°)$ in Fig. 14.

Consequently, a Gaussian distribution may not provide a realistic approximation to describe the effects of roughness, even in the case of a uniform roughness as modeled here.

All these density functions exhibit very close values for the most probable value of the density function and the average value $\langle P_l \rangle_n$, and also the median value. That means that the closeness of the values of the most probable value, the average value and the median value do not imply the symmetry of the density function, although the near equality of the most probable value and the average value reflects certainly that the law of abrasion applied is a uniform law.

The fact that the most probable value nearly equals the average value of the density function demonstrates the possibility of taking, to a first order, the average value as the mean indicator of the effect of roughness on polarization.

Whereas the polarization of a sphere is symmetrical with respect to the angle $\theta_s = 180°$ and is invariant through a ϕ_s rotation, we find that the density functions are not symmetrical with respect to $\theta_s = 180°$ (see Fig. 17 to Fig. 19), and are very different for the three values of ϕ_s (given θ_s) (see Figs. 14 – 15). However, the value of the first maximum (which is considered as the mean effect of roughness on polarization) is kept the same for a fixed θ_s. It is also symmetrical with respect to $\theta_s = 180°$. Thus, over all the simulations (n=1000), whatever the scattering angles, the mean value of the density functions follows exactly the symmetry of a sphere.

Any value of the polarization different to the first maximum will not be preserved for different ϕ_s, given θ_s. Indeed, the polarization obtained with a rough sphere for a specific scattering

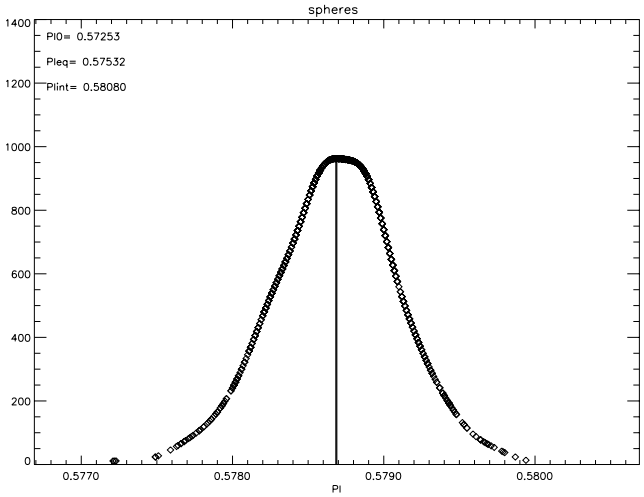

Fig. 9. Density function of linear polarization P_l for $(\theta_s = 60^\circ, \phi_s = 0^\circ)$. The vertical lines correspond to $\langle P_l \rangle_n$ and the median value.

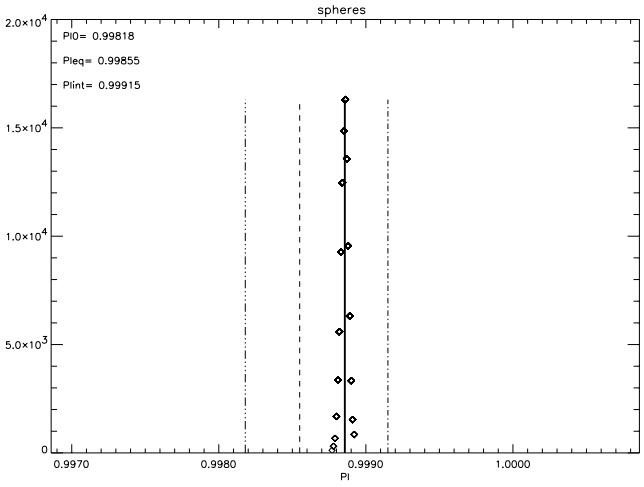

Fig. 10. Density function of linear polarization P_l for $(\theta_s = 90^\circ, \phi_s = 0^\circ)$. $P_{l,0}$:$-\cdots-$, $P_{l,\mathrm{eq}}$:$--$, $P_{l,\mathrm{int}}$:$-\cdot-$. The vertical lines correspond to $\langle P_l \rangle_n$ and the median value.

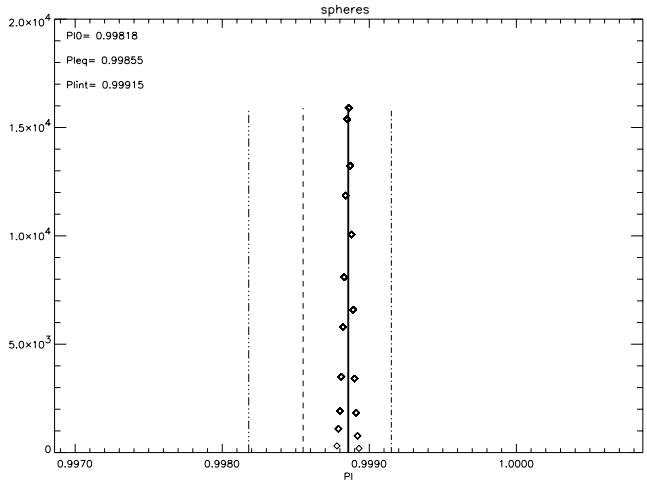

Fig. 11. Density function of linear polarization P_l for $(\theta_s = 90^\circ, \phi_s = 90^\circ)$. $P_{l,0}$:$-\cdots-$, $P_{l,\mathrm{eq}}$:$--$, $P_{l,\mathrm{int}}$:$-\cdot-$. The vertical lines correspond to $\langle P_l \rangle_n$ and the median value.

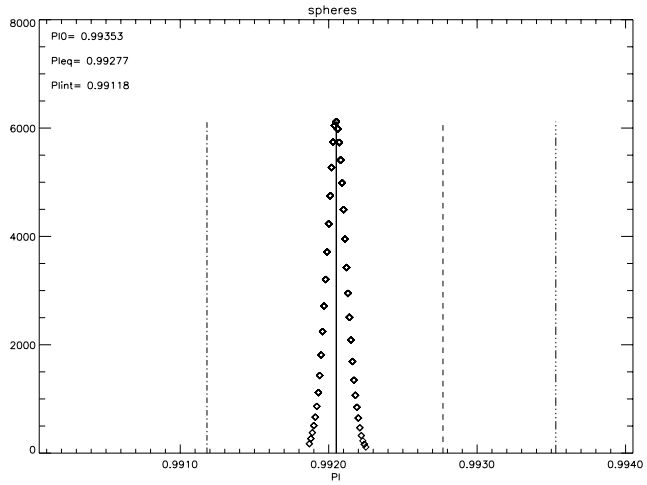

Fig. 12. Density function of linear polarization P_l for $(\theta_s = 95^\circ, \phi_s = 0^\circ)$. $P_{l,0}$:$-\cdots-$, $P_{l,\mathrm{eq}}$:$--$, $P_{l,\mathrm{int}}$:$-\cdot-$. The vertical lines correspond to $\langle P_l \rangle_n$ and the median value.

angle (θ_s,ϕ_s) has no reason to be equal to the polarization for another couple (θ_s,$\phi_s^{'}$) because of the anisotropy of the rough sphere to the incident light. This explains why the graphs of the density function are not identical for different values of ϕ_s (for a fixed θ_s), and also means that the density functions accurately contain the information on the dependence of the polarization on the anisotropy of the rough sphere, due to its roughness.

As a first conclusion, we can say that the mean value of the density function represents the *average* effect of roughness on polarization.

The secondary maximum which appears in some cases suggests the coexistence of two effects of roughness on polarization.

We have calculated, using Mie's theory, the linear polarization of the equivalent sphere, i.e., the sphere that would have the same number of dipoles: $P_{l,\mathrm{eq}}$, and, the linear polarization $P_{l,\mathrm{int}}$ for the interior sphere of radius $0.9\,a_{\mathrm{eff}}$. The interior sphere corresponds to the initial sphere from which all the dipoles of the surface have been removed (see Fig. 3 and Sect. 3.2). All the graphs of the density function also show the value $P_{l,0}$ of the linear polarization of the initial sphere of radius $a_{\mathrm{eff}} = 0.3\mu$m, and the average value $\langle P_l \rangle_n$ and the median value, both pointed out by vertical lines.

Fig. 20 shows the variation of the polarization for the equivalent sphere and the interior sphere related to those for the initial sphere versus the scattering angle θ_s, so that the values for the initial sphere are represented by the horizontal line $y = 0$. Fig. 20 also shows the most probable values obtained from the density functions for each angle where they have been calculated. Fig. 20 represents the effect of small variations of the volume of spheres on polarization. The values plotted for the three sphere ($P_{l,0}, P_{l,\mathrm{eq}}, P_{l,\mathrm{int}}$) have been calculated using Mie's theory.

Fig. 20 clearly shows that the polarization of the rough sphere given by the most probable value of the density function

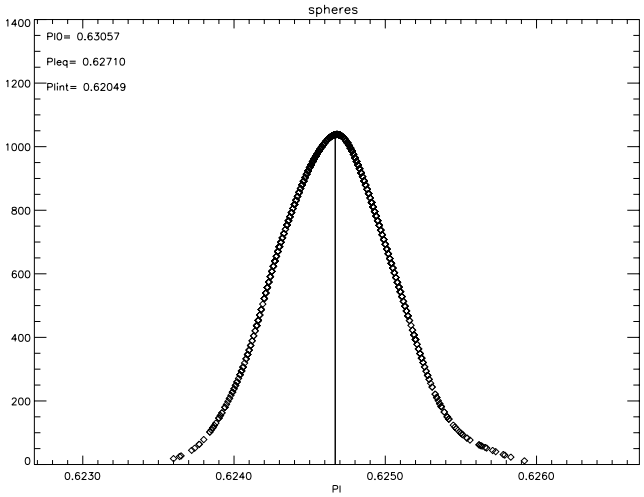

Fig. 13. Density function of linear polarization P_l for ($\theta_s = 120°, \phi_s = 0°$). The vertical lines correspond to $\langle P_l \rangle_n$ and the median value.

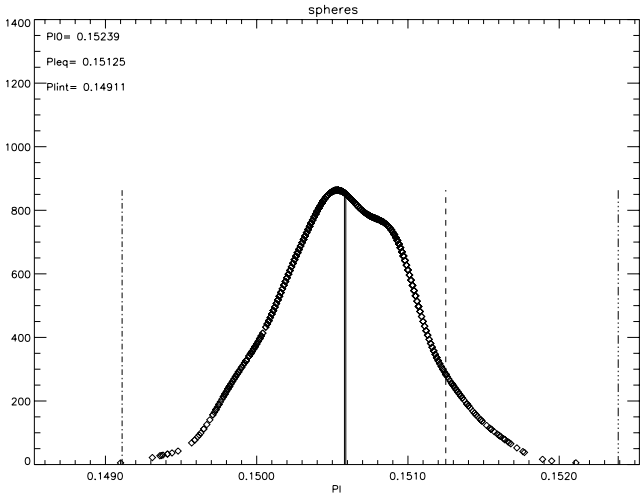

Fig. 14. Density function of linear polarization P_l for ($\theta_s = 150°, \phi_s = 0°$). $P_{l,0}$:$-\cdots-$, $P_{l,\mathrm{eq}}$:$--$, $P_{l,\mathrm{int}}$:$-\cdot-$. The vertical lines correspond to $\langle P_l \rangle_n$ and the median value.

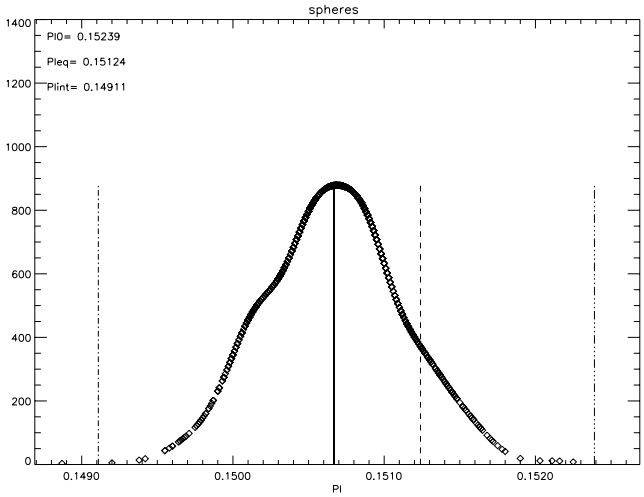

Fig. 15. Density function of linear polarization P_l for ($\theta_s = 150°, \phi_s = 90°$). $P_{l,0}$:$-\cdots-$, $P_{l,\mathrm{eq}}$:$--$, $P_{l,\mathrm{int}}$:$-\cdot-$. The vertical lines correspond to $\langle P_l \rangle_n$ and the median value.

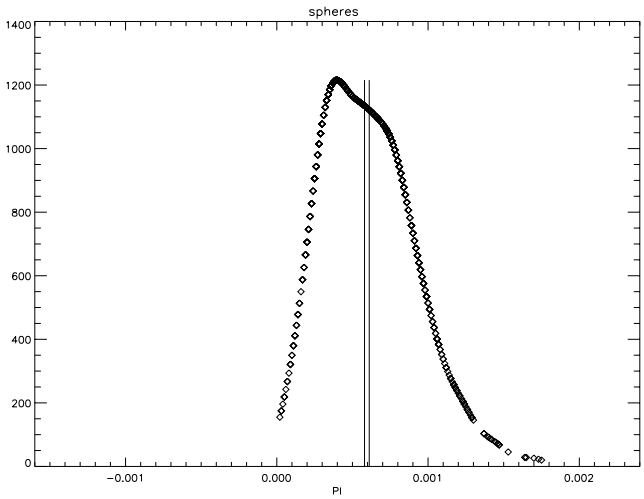

Fig. 16. Density function of linear polarization P_l for ($\theta_s = 180°, \phi_s = 0°$). $P_{l,0} = P_{l,\mathrm{eq}} = P_{l,\mathrm{int}} = 0$. The vertical lines correspond to $\langle P_l \rangle_n$ and the median value.

behaves like a sphere with some "*effective*" radius. Together with the spherical symmetry of the most probable value, this implies that this value mirrors the main information about the polarization of the rough sphere due to its volume. Thus, we can say that the polarization of a sphere due to roughness can be characterized by an *effective* polarization equal to the mean value of the density functions for each scattering angle.

Although neither of the equivalent sphere nor the interior sphere correctly approximate the rough sphere, the interior sphere seems to provide a better approximation of the rough sphere. Moreover, whereas the equivalent sphere represents a sphere of equal mass, this study shows that, since the *effective* polarization of a rough sphere as a function of angle follows a variation of the volume, the polarization of the interior sphere corresponds better to the polarization of a rough sphere. Thus, the *effective* polarization of the rough sphere could be considered as the sum of the polarization of the interior sphere plus a correction which would correspond to the rough surface, so that the sum is equal to the mean values of the density functions for each angle.

Thus, we attribute the most probable value of the density function mainly to the effect of the global volume of the rough sphere, characterizing only the average effect of roughness. Similarly, we attribute the secondary maximum to the details of roughness and the dependence of the polarization on the anisotropy of the grain with the scattering angle.

Among the density functions Figs. 5 to 16, we note that near the scattering angle $\theta_s = 90°$, the density function is very symmetrical and narrow about the most probable value and is also clearly unimodal. The shape of the density function near $\theta_s = 90°$ does not depend on ϕ_s. This implies that for the

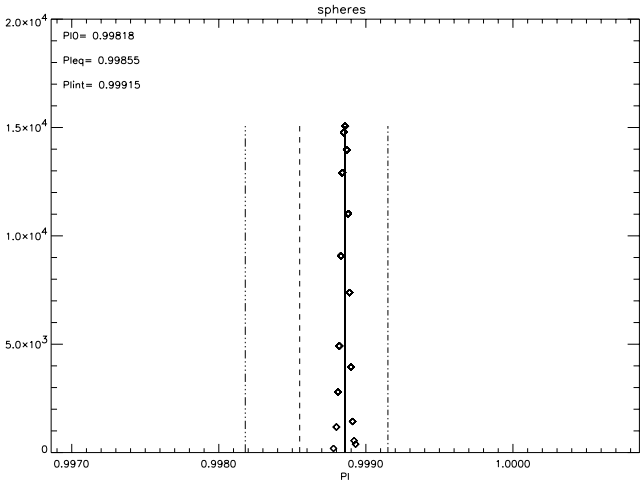

Fig. 17. Density function of linear polarization P_l for ($\theta_s = 270^\circ, \phi_s = 0^\circ$). $P_{l,0}$:$-\cdots-$, $P_{l,\mathrm{eq}}$:$--$, $P_{l,\mathrm{int}}$:$-\cdot-$. The vertical lines correspond to $\langle P_l \rangle_n$ and the median value.

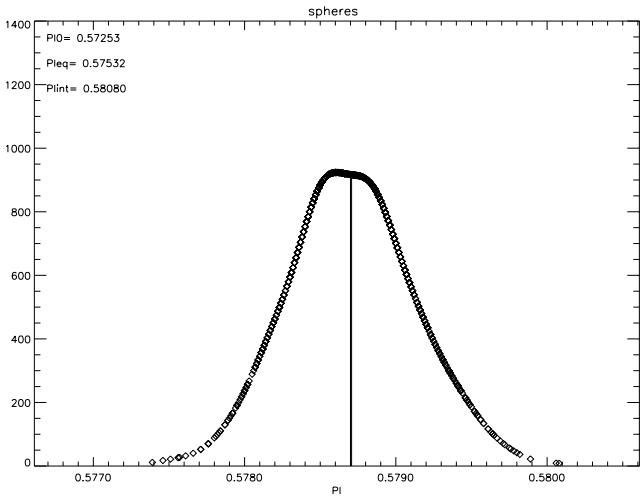

Fig. 18. Density function of linear polarization P_l for ($\theta_s = 300^\circ, \phi_s = 0^\circ$). The vertical lines correspond to $\langle P_l \rangle_n$ and the median value.

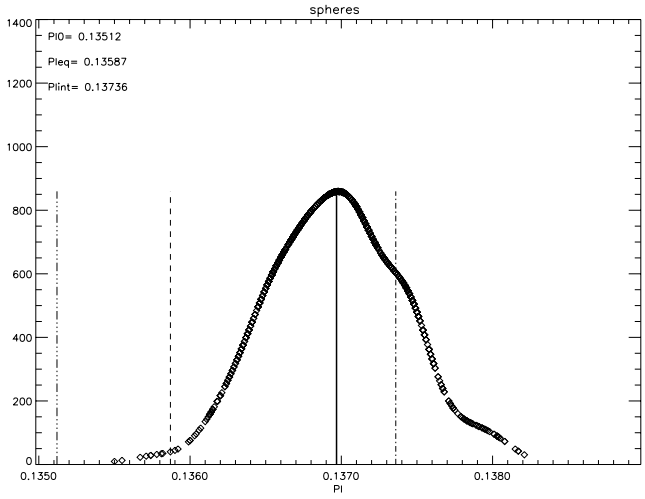

Fig. 19. Density function of linear polarization P_l for ($\theta_s = 330^\circ, \phi_s = 0^\circ$). $P_{l,0}$:$-\cdots-$, $P_{l,\mathrm{eq}}$:$--$, $P_{l,\mathrm{int}}$:$-\cdot-$. The vertical lines correspond to $\langle P_l \rangle_n$ and the median value.

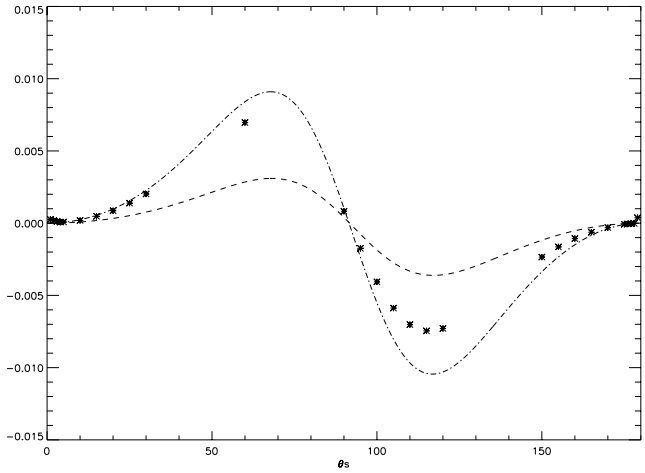

Fig. 20. Variation of the polarization of the different spheres related to the polarization of the initial one ($P_{l,0}$, represented by $y = 0$) versus θ_s. $P_{l,\mathrm{eq}}$:$--$, $P_{l,\mathrm{int}}$:$-\cdot-$, $\langle P_l \rangle_n$:$*$

values of the scattering angle near $\theta_s = 90^\circ$, the polarization is not sensitive to the type of roughness.

Moreover, in Fig. 20, we can see that even the average effect of roughness is small compared to the polarization of the initial sphere Pl_0. At this angle, we cannot distinguish between any of the three spheres: $\langle P_l \rangle_n$, $P_{l,\mathrm{eq}}$, $P_{l,\mathrm{int}}$.

In conclusion, near $\theta_s = 90^\circ$, the polarization is probably mostly due to the overall shape of the grain, and more precisely to the geometrical symmetry of the global volume related to the incident light. Thus, at $\theta_s \simeq 90^\circ$, the polarization is not affected by roughness of grains and only depends on the general characteristics of the volume of the grain. Thus, $\theta_s \simeq 90^\circ$ is not the best angle to observe effects of roughness on polarization.

Kozasa et al. (1993) have also observed that for non-absorbing small particles the maximum of linear polarization (which is obtained near $\theta_s \simeq 90^\circ$) is more closely related to the chemical composition of the particle than to its structure. Nevertheless, Perrin & Sivan (1991) have observed a small shift of the maximum of polarization near $\theta_s = 90^\circ$. This could be explained by the fact that as they modeled roughness deep into the grain, this kind of roughness may affect the geometrical volume of the grain, as in porous grains, and then modify significantly the observed polarization. Indeed, their polarization curves for porous grains are very similar to those for rough grains.

In the same paper, they also observed that the effect of roughness increases the amount of scattered light I_s for $\theta_s > 100^\circ$, and decreases I_s for $\theta_s < 100^\circ$. This will be reflected into the degree of polarization by an opposite effect (see definition of P_l in Sect. 3) which is visible in Fig. 20.

From this paper, it also follows that approximations by spheres with equivalent mass correspond to neither rough grains nor porous grains. This is in agreement with Fig. 20, where the variation of polarization due to roughness follows changes of

volume and not to changes of mass (which would correspond to the sphere of equivalent mass $P_{l,\mathrm{eq}}$).

With our statistical approach (with $n = 1000$ simulations), the accuracy of the results for the most probable value, and then the average value $\langle P_l \rangle_n$, is found to about $10^{-3}\%$ which is very accurate. However, the actual accuracy of measurements does not give access to measurements of the effects of this degree of roughness on polarization. The greatest effect we have obtained for $\theta_s = 60^\circ$ gives $|\langle P_l \rangle_n - Pl_0| \simeq 0.6\%$ while very accurate observations (Aitken et al. 1997) are obtained within 0.5%. Recent experimental results (Worms et al. 1999) lead to an error of about $1-3\%$, which depends on the intensity I_s received and on θ_s since the light is not scattered isotropically. Nevertheless, such effects of roughness, with such size parameter of grains, could be detectable for some angles in the future.

5. Conclusions and perspective

This statistical study leads to the probability density functions of the linear polarization for various scattering angles. The probability density function characterizes the state of roughness of grains. Indeed, since this density function depends on the law of abrasion applied to the grain, it contains information on the type of erosion which the grains have undergone.

We found that the first maximum of the density function, which corresponds to the most probable value, nearly equals the average value of the function. We think that this is in close relation with the random law of abrasion. However, the density function is symmetrical with respect to neither the most probable value nor the average value, and furthermore it sometimes shows a secondary maximum. Consequently, the details of the density functions show the dependence of the polarization on the overall geometrical shape of grains (in the present case, on their roughness). Moreover, this study shows that the law of dependence of the polarization on the shape of grains cannot be described by a simple Gaussian distribution, even in the case of a uniform roughness.

The mean indicator of the effect of roughness is the most probable value. Nevertheless, the closeness of the most probable value and the average value leads us to interpret the most probable value as the *average* effect, or global effect, of roughness on polarization.

According to the variations of the most probable value with the scattering angle (Fig. 20), we conclude that the rough sphere still behaves like a sphere. We conclude that roughness does not destroy the general properties of polarization, which are essentially due to the global volume of the grain, i.e. its geometrical shape, relative to the incident light.

The effects of roughness are important around $\theta_s \simeq 60^\circ$ and negligible near $\theta_s \simeq 90^\circ$ (Fig. 20, see also the density functions). Indeed, the density functions at $\theta_s = 90^\circ$ and 95° are very narrow and symmetrical about the most probable value. At $\theta_s = 90^\circ$, the effects of roughness could be approximated by a Dirac function. We conclude that the effect of volume is major near $\theta_s \simeq 90^\circ$, and that this angle is adequate to study in particular these kind of effects, for example, those of porous grains on polarization.

Finally, we explain the shape of the density function, in particular the secondary maximum, by the coexistence of two effects on polarization: the first and most important one associated with the most probable value of the density function comes from the general shape of the grain, (its geometrical volume), and the second one, associated with the secondary maximum, is attributed to the state of roughness of the grain. We emphasize that these two effects could have been separated only through the probability density function of polarization.

Neither the mass equivalent sphere nor the interior sphere fit the polarization of the rough sphere. Nevertheless, since the interior sphere seems to be a better approximation of the rough sphere (Fig. 20), together with the fact that the behavior of the polarization for a rough sphere is that of a sphere, we suggest that effects of roughness on polarization could be approximated by an *effective* polarization. This *effective* polarization could be composed of a mean part deduced from the interior sphere, and a correction which corresponds to the roughness, so that the sum of both is given by the most probable value of the density function of polarization for each scattering angle.

All these preliminary results were obtained with a purely scattering grain of water ice. In a following paper, we will apply this method to study the effect of roughness when water ice is absorbing, in particular at the wavelength $\lambda = 3.1\,\mu$m. In addition, as we observe not only one grain but a collection of grains in circumstellar medium, a forthcoming paper will discuss a collection of randomly oriented grains, again with this kind of approach using a kernel method.

We also plan to analyze the evolution of the secondary maximum with the degree of roughness. To achieve this, we intend to increase the degree of roughness modeled, still with a uniform law, until all the dipoles of the shell constituting the surface are removed, i.e. until the final grain is in fact the interior sphere.

A more general goal is, of course, to get more information about the effect of morphology and internal structure of grains on polarization. However, we consider that a complete and careful study of roughness on polarization is a necessary step before dealing with complex shapes of grains, such as fractals, where effects of external morphology and internal structure are mixed (as already mentioned by Ossenkopf (1991)).

Appendix A: The Gaussian kernel method

Consider a sample $\mathbf{X_n}$ of size n: $(X_1 \cdots X_n)$ of identically distributed, independent random variables. We intend to provide an estimate of the probability density function of the generic variable X, namely $f(x)$, defined by the property:

$$P(x \in [a,b]) = \int_a^b f(x)dx \tag{A.1}$$

If we estimate the probability density function through the derivative of the empirical repartition function, we obtain a sum of Dirac functions.

However, if we convolute these Dirac functions by a kernel $K(x)$ which has 'good' properties, the function obtained is then a continuous function and an estimator of the probability density function (Devroye 1986). The estimator of the density function of the sample $\mathbf{X_n}$ is denoted $f_{\mathbf{X_n}}(x)$, and is given, after convolution, by:

$$f_{\mathbf{X_n}}(x) = \frac{1}{n}\sum_{i=1}^{n}\frac{1}{h_n}K(\frac{x-X_i}{h_n}), \quad (A.2)$$

$$\equiv \frac{1}{n}\sum_{i=1}^{n}K_{h_n}(x-X_i), \quad (A.3)$$

where h_n is a parameter which is fixed with the choice of the kernel applied. This parameter is used to smooth the shape of the curve, so that h_n has to tend to zero when n goes to infinity, but not too fast:

$$\lim_{n\to\infty} nh_n \longrightarrow \infty. \quad (A.4)$$

The 'good' properties of $K(x)$ are:

$$\lim_{|x|\to\infty}|x|K(x)=0, \qquad \int_{-\infty}^{\infty}K(x)dx=1, \quad (A.5)$$

which ensure the convergence of $f_{\mathbf{X_n}}(x)$ in probability to the true density function $f_X(x)$ of the random variable X. Therefore:

$$\int K_{h_n}(x-u)f_{\mathbf{X_n}}(u)du = (K_{h_n} * f_{\mathbf{X_n}})(x) \longrightarrow f_X(x) \quad h_n \to 0 \quad (A.6)$$

A useful kernel is the Gaussian kernel which, moreover, has the property to be C^∞:

$$K(\frac{x-X_i}{h_n}) = \frac{1}{\sqrt{2\pi}}\exp(-((x-X_i)/h_n)^2/2) \quad (A.7)$$

where $h_n = \dfrac{1.059\,\sigma}{n^{1/5}}$, and σ is the standard deviation.

In our case, $n = 1000$, and $X \equiv P_l$.

Acknowledgements. We wish to thank Pr. M. Broniatowski (Université Paris VI, Laboratoire de Statistique Théorique et Appliquée) for useful discussions and help regarding the computations and presentation of the Gaussian kernel method. We thank the referee for his many helpful comments. We also thank B.T. Draine and P.J. Flatau for providing the DDSCAT.5a9 program.

References

Aitken D.K., Smith C.H., Moore T.J.T., et al., 1997, MNRAS 286, 85
Bohren C.F., Huffman D.R., 1983, Absorption and Scaterring of Light by Small Particle, Wiley-Interscience
Devroye L., 1986, A Course in Density Estimation, Dirkhauser
Draine B.T., 1988, ApJ 333, 848
Draine B.T., Flatau P.J., 1994, J. Opt. Soc. Am. A 11(4), 1491
Draine B.T., Goodman J., 1993, ApJ 405, 685
Draine B.T., Weingartner J.C., 1997, ApJ 480, 633+
Drossart P., 1990, ApJ 361, L29
Hagen W., Greenberg, J.M., Tielens, A.G.G.M., 1983, A&A 117, 132
Kozasa T., Blum J., Okamoto H., Mukai T., 1993, A&A 276, 278
Lafon J.P.J., Berruyer N., 1991, A&AR 2, 249
Lumme K., Rahola J., 1994, ApJ 425, 653
Mathis J.S., Rumpl W., Nordsieck K.H., 1977, ApJ 217, 425
Mathis J.S., Whiffen G., 1989, ApJ 341, 808
McGuire A.F., Hapke B.W., 1995, Icarus 113, 134
Mishchenko M.I., Hovenier J.W., 1995, Opt. Lett. 20(12), 1356
Mugnai A., Wiscombe W., 1980, J. Almos. Sci. 37, 1291
Muinonen K., 1996, Earth, Moon, Planets 72, 339
Muinonen K., 1998, A&A 332, 1087
Muinonen K., Lagerros J.S.V., 1998, A&A 333, 753
Ossenkopf V., 1991, A&A 251, 210
Ossenkopf V., 1993, ApJ 280, 617
Peltoniemi J.I., Lumme K., Muinonen K., Irvine, W.M., 1989, Appl. Opt. 28(19), 4088
Pendleton Y.J., Tielens A.G.G.M., Werner M.W., 1990, ApJ 349, 107
Perrin J.M., Sivan J.P., 1991, ApJ 247, 497
Pollack J.B., Hollenback D., Beckwith S., et al., 1991, ApJ 247, 497
Purcell E.M., Pennypacker C.R., 1973, ApJ 186, 705
Rouleau F., 1996, ApJ 310, 686
Schiffer R., 1985, A&A 148, 347
Stognienko R., Henning T., Ossenkopf V., 1995, ApJ 296, 797+
Wolff M.J., Clayton G.C., Gibson S.J., 1998, ApJ 503, 815
Wolff M.J., Clayton G.C., Martin P.G., Schulte-Ladbeck R.E., 1994, ApJ 423, 412
Worms J.C., Renard J.B., Hadamcik E., Levasseur-Regourd A.C., Gayet J.F., 1999, Icarus 142, 281